Effects of S-Se substitution and magnetic field on magnetic order in $Fe_{0.5}Ti(S,Se)_2$ layered compounds

A.F. Gubkin[a,b,*], E.M. Sherokalova[b], L. Keller[c], N.V. Selezneva[b], A.V. Proshkin[a,b], E.P. Proskurina[b], N.V. Baranov[a,b,**]

[a] *Institute of Metal Physics, Russian Academy of Science, 620990, Yekaterinburg, Russia*
[b] *Institute of Natural Science, Ural Federal University, 620083, Yekaterinburg, Russia*
[c] *Laboratory for Neutron Scattering, Paul Scherrer Institut (PSI), CH-5232 Villigen, Switzerland*

Abstract

Powder neutron diffraction and specific heat measurements have been employed to study the evolution of an antiferromagnetic (AFM) structure in the intercalated $Fe_{0.5}TiS_{2-y}Se_y$ compounds with S-Se substitution and under application of a magnetic field. In $Fe_{0.5}TiS_2$ ($y = 0$), the magnetic structure just below $T_N \simeq 140\,K$ is incommensurate while it becomes commensurate with further cooling below $T_t \simeq 125\,K$. The presence of two magnetic phase transitions at T_t and T_N in $Fe_{0.5}TiS_2$ is confirmed by specific heat measurements. The field-induced AFM–FM transitions occurring in $Fe_{0.5}TiS_2$ within temperature interval $T_t < T < T_N$ and below T_t are evidenced by neutron diffraction measurements under application of a magnetic field. Unlike $Fe_{0.5}TiS_2$ having a quadruplicated AFM structure, the compounds with the Se concentrations $y > 0.5$ are observed to exhibit an AFM structure with the doubled magnetic unit cell along a and c crystallographic directions of the monoclinic crystal lattice ($I12/m1$ space group). In the transition region around the critical Se concentration $y_c \approx 0.5$, the magnetic structure of $Fe_{0.5}TiS_{2-y}Se_y$ is found to be incommensurate. The appearance of the AFM order with decreasing temperature in $Fe_{0.5}TiS_{2-y}Se_y$ is accompanied by anisotropic deformations of the crystal lattice. At low temperatures, the

*Corresponding author
**Principal corresponding author
Email addresses: agubkin@imp.uran.ru (A.F. Gubkin), baranov@imp.uran.ru (N.V. Baranov)

Fe magnetic moments in all $Fe_{0.5}TiS_{2-y}Se_y$ form an angle $14^\circ - 16^\circ$ to the c crystallographic direction, which can be ascribed to the crystal field effects and spin-orbital couplings.

Keywords:
Magnetically ordered materials, Phase transitions, Heat capacity, Exchange and superexchange, Neutron diffraction
PACS: 75.25.-j, 75.50.Bb, 75.50.Ee

---

1. Introduction

Some transition metal (T) dichalcogenides M_xTX_2 (X = chalcogen) intercalated with open shell $3d$-metal (M) atoms are observed to exhibit a long-range magnetic order of various kinds at high intercalant concentrations ($x \geq 0.25$) [1, 2]. The intercalation of guest (M) atoms into TX_2 matrixes is possible owing to the presence of a weak coupling between X-T-X tri-layers via van der Waals forces. The presence of a three-dimensional magnetic order in highly intercalated M_xTX_2 compounds is associated with the indirect exchange interaction between $3d$ electrons of M atoms via conduction electrons of the Ruderman-Kittel-Kasuya-Yoshida (RKKY) type together with the superexchange interaction through chalcogen atoms [2, 3, 4, 5]. The T atoms are suggested to be also involved into interlayer exchange interactions through M-T-M path, which is supported by neutron diffraction data [6], X-ray spectroscopy experiments and electronic structure calculations [5]. The magnetic properties of highly intercalated M_xTX_2 compounds are controlled by combination of reduced dimensionality, ordering effects of intercalated M atoms, magnetocrystalline anisotropy and exchange interactions of different types. Thus, the neutron diffraction measurements have revealed the presence of a helimagnetic ground state with a period of about 480 Å in $Cr_{0.33}NbS_2$ [7], while $Cr_{0.33}NbSe_2$ is reported to be a ferromagnet [8]. As is shown recently [9], the phase transition from a chiral antiferromagnetic (AFM) structure to the collinear ferromagnetic (FM) state in $Cr_{0.33}NbS_2$ occurs via formation of chiral soliton lattice with controllable parameters, which opens new possibilities for application in spintronic devices. The presence of different magnetic states has been revealed in Cr intercalated compounds $Cr_{0.5}TiSe_2$ [10] and $Cr_{0.5}TiTe_2$ [11] which exhibit incommensurate AFM structure and FM ordering, respectively. These observations indicate that not only the type and concentration of inserted M atoms but also the

type of TX_2 matrixes affects the magnetic order in the intercalated compounds. Moreover, the properties of TX_2 and M_xTX_2 compounds are found to be very sensitive to applied pressure [12, 13, 14, 15]. In particular, as was shown recently for $Co_{0.33}NbS_2$ [16], high pressure substantially modifies the electrical properties and reduces the Neel temperature of this compound ($dT_N/dP \sim -1\,\mathrm{K/kbar}$).

In the present work, we study the changes in magnetic structures of $Fe_{0.5}TiS_{2-y}Se_y$ compounds caused by the S-Se isoelectronic substitution suggesting that such a substitution will produce a negative chemical pressure because of the difference of sulfur and selenium ionic radii. Unlike above mentioned Cr intercalated transition metal dichalcogenides both the non-substituted compounds $Fe_{0.5}TiS_2$ and $Fe_{0.5}TiSe_2$ are antiferromagnets with close values of the Neel temperatures ($\simeq 140\,\mathrm{K}$) [6, 17]. However, $Fe_{0.5}TiS_2$ based on the titanium disulfide exhibits an AFM structure with a quadruplicated magnetic unit cell along a and c directions relative to the crystal unit cell [17], while the magnetic structure of $Fe_{0.5}TiSe_2$ based on the titanium diselenide has an AFM structure with in twice reduced periodicity [6]. Below the Neel temperature $T_N \simeq 140\,\mathrm{K}$, application of a magnetic field above the critical value H_c induces in $Fe_{0.5}TiS_2$ a metamagnetic AFM–FM phase transition [17]. This phase transition is accompanied by large magnetoresistance effect ($|\frac{\Delta\rho}{\rho}|$ up to 30 %) and hysteresis which increases with decreasing temperature. Below 110 K, the field-induced AFM–FM transition in $Fe_{0.5}TiS_2$ becomes irreversible. This makes the magnetic behavior of $Fe_{0.5}TiS_2$ rather unique, since despite the presence of an AFM ground state it behaves as a permanent magnet with coercive fields up to 50 kOe at low temperatures [17].

In this article, together with zero field neutron powder diffraction (NPD) data obtained on $Fe_{0.5}TiS_{2-y}Se_y$ samples ($0 \leq y \leq 2$) in a wide temperature range we present the results of NPD measurements in applied magnetic fields in order to reveal the evolution of the magnetic structure at the field-induced AFM–FM transition and metastability effects. The specific heat measurements were performed as well in order to characterize the changes in magnetic states with temperature.

2. Experimental details

$Fe_{0.5}TiS_{2-y}Se_y$ compounds with $y = 0, 0.5, 1, 1.5, 2$ were prepared by solid state chemical reaction. A detailed description of the procedure can be found elsewhere [17]. The obtained samples were examined by powder X-ray diffrac-

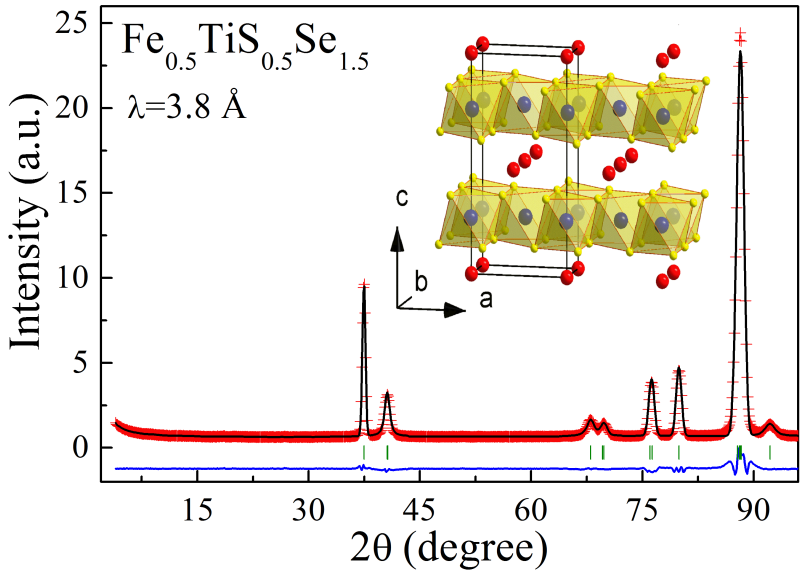

Figure 1: (Colour on-line) The best fit result on the NPD pattern for $Fe_{0.5}TiS_{0.5}Se_{1.5}$ sample at room temperature. Symbols are experimental values of the intensity, and lines represent the results of the fit. The difference between calculated and observed intensities is shown at the bottom. The row of vertical marks below the patterns refers to the nuclear Bragg peaks.

tion analysis using a Bruker D8 Advance diffractometer with CuKα radiation. The neutron powder diffraction (NPD) measurements were performed using DMC diffractometer at the Spallation Source SINQ, Switzerland with neutron wavelength 3.8 Å. For $Fe_{0.5}TiS_2$ the NPD measurements in applied magnetic fields up to 28 kOe were carried out on a cylindrical sample compacted from the powdered compound. Possible spin configurations compatible with the lattice symmetry were obtained with recent version of the *SARAh* program [18]. The Rietveld refinement of the crystal and magnetic structures has been done by means of the FULLPROF [19] software. The specific heat measurements were performed by using an adiabatic calorimeter and by a Quantum Design PPMS.

3. Results and discussion

3.1. Crystal structure of $Fe_{0.5}TiS_{2-y}Se_y$

The crystal structure and phase purity of $Fe_{0.5}TiS_{2-y}Se_y$ powder samples with $y = 0, 0.5, 1, 1.5, 2$ were checked by x-ray and neutron diffraction mea-

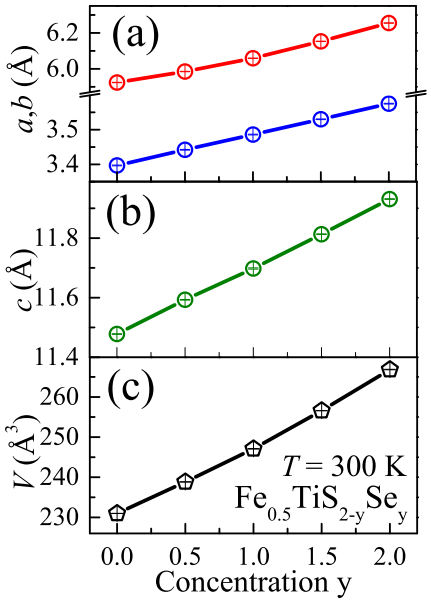

Figure 2: (Colour on-line) Concentration dependencies of the unit cell parameters a, b, c and unit cell volume V estimated for $Fe_{0.5}TiS_{2-y}Se_y$ compounds at room temperature.

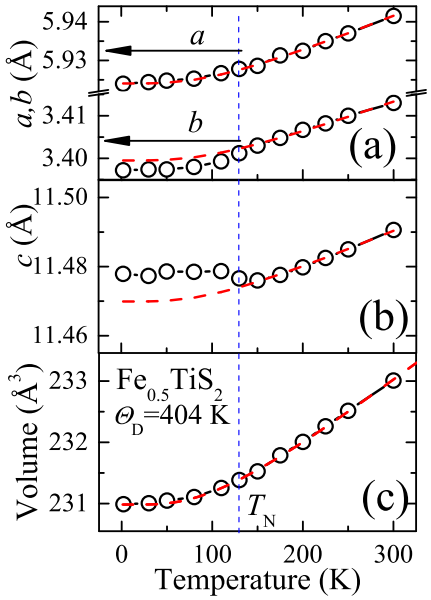

Figure 3: (Colour on-line) Temperature dependencies of the unit cell parameters a, b, c and unit cell volume V for $Fe_{0.5}TiS_2$. The red dashed line through the symbols represents theoretical curve calculated within the GD model.

surements at room temperature. The crystal structure of all compounds has been identified as a monoclinic of the Cr_3S_4-type (space group $I12/m1$) with the lattice parameters which correspond to the $a_0\sqrt{3}\times a_0\times 2c_0$ super-structure (where a_0 and c_0 refer to the primitive hexagonal unit cell of the NiAs structure). Ti atoms occupy $4i$ Wyckoff site in the centers of the octahedrons which are formed by S/Se atoms randomly distributed over two $4i$ Wyckoff positions while Fe atoms occupy $2a$ Wyckoff site (see inset in the Fig. 1). The best fit result for the room temperature NPD pattern of $Fe_{0.5}TiS_{0.5}Se_{1.5}$ sample is shown at Fig. 1. The refined structural parameters are well agree with the previously published data for $Fe_{0.48}TiSe_2$ and $Fe_{0.5}TiS_2$ [17, 20, 21].

The thermal and concentration dependencies of the unit cell parameters were obtained from the Rietveld refinement of the NPD patterns measured in the temperature range 2 K - 300 K for all the studied $Fe_{0.5}TiS_{2-y}Se_y$ compounds. According to the room temperature data, the substitution of Se for S leads to the nearly linear growth of the lattice parameters and unit cell volume (see Figs. 2(a)-(c)). Such an expected behavior obviously originates from the larger ionic radius of selenium in comparison with sulfur. The temperature dependencies of the unit cell parameters for $Fe_{0.5}TiS_2$ are displayed in Figs. 3(a) - (c). Above the Neel temperature $T_N \simeq 140$ K the lattice thermal expansion can be well approximated by the Grüneisen-Debye (GD) theory with the Debye temperature $\Theta_D = 404$ K, while below T_N a clear deviation of the unit cell parameters from the theoretical curves is observed. As follows from Fig. 3(a), unlike the $a(T)$ dependence which quite well follows the expected phononic thermal expansion, the $b(T)$ curve deviates down from the GD line below T_N while the $c(T)$ curve shows an opposite behavior. As to the temperature dependence of the unit cell volume $V(T)$, it well obeys the GD theory. These results show that the magnetic ordering in $Fe_{0.5}TiS_2$ below 140 K is accompanied by anisotropic magnetoelastic deformations of the crystal lattice. Similar behavior was previously reported for $Fe_{0.5}TiSe_2$ [6, 22] and may be interpreted in terms of a single ion model with the presence of the spin-orbit interaction and the crystal field effect.

3.2. Magnetic structure of $Fe_{0.5}TiS_2$

The magnetic structure of $Fe_{0.5}TiS_2$ as a function of temperature and applied magnetic field was studied using high intensity neutron diffraction data measured on DMC diffractometer (PSI, Switzerland). As shown in Fig. 4, on cooling below the Neel temperature, a set of additional magnetic reflections forbidden by the symmetry rules of the $I12/m1$ space group appears at the

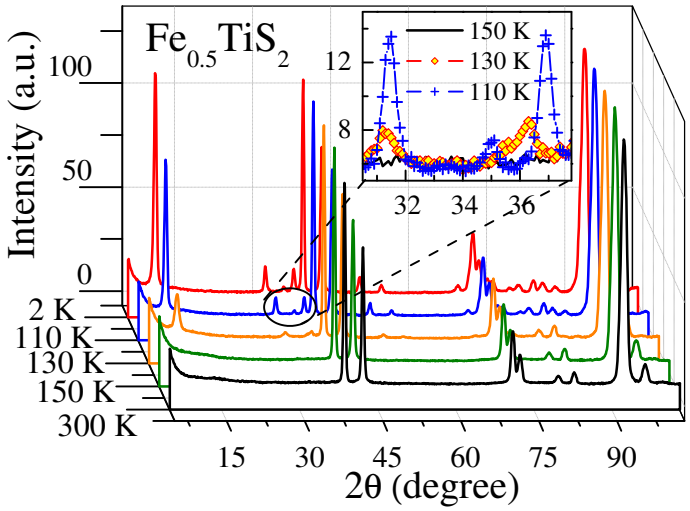

Figure 4: (Colour on-line) Evolution of the neutron diffraction patterns versus temperature as a 3D plot for $Fe_{0.5}TiS_2$. Inset shows the AFM reflections around $2\theta = 34°$ measured below and above $T_t \simeq 125\,K$.

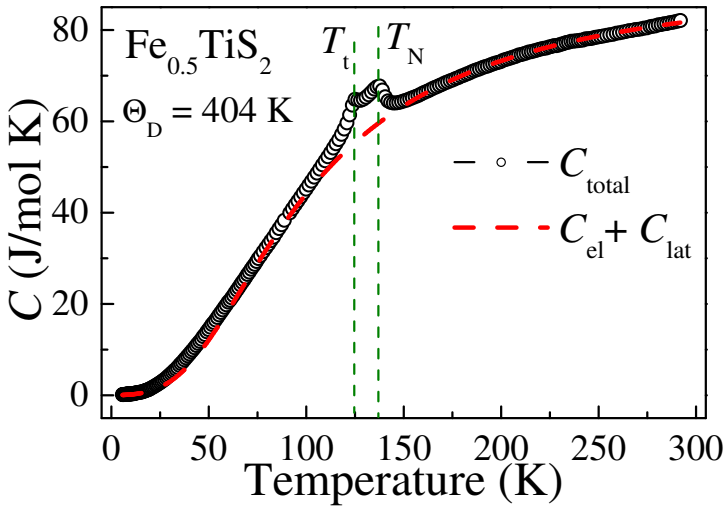

Figure 5: (Colour on-line) Temperature dependence of the specific heat for $Fe_{0.5}TiS_2$. Red dashed line shows electronic and lattice contributions. (*see text for details*).

NPD pattern measured at $T = 130\,\mathrm{K}$ relative to those observed above the Neel temperature. This is in agreement with the recently reported results of magnetic measurements [17] which revealed a second order transition from paramagnetic state to antiferromagnetic state at $T_\mathrm{N} \simeq 140\,\mathrm{K}$. The magnetic peaks observed at $T = 130\,\mathrm{K}$ can be indexed with the propagation vector $\mathbf{k} = (\mu, 0, \nu)$, where $\mu = 0.26$ and $\nu = 0.23$ suggest the incommensurate (ICM) magnetic structure. Both μ and ν values evolve on cooling below 130 K and lock in to the commensurate (CM) value $\mu = \nu = 0.25$ at $T = 110\,\mathrm{K}$ (see the inset in Fig. 4). Assuming that such a change of the magnetic structure below 130 K occurs through a phase transition we have performed the measurements of the specific heat of $Fe_{0.5}TiS_2$ in order to check this assumption. Indeed, as can be seen from Fig. 5, the $C(T)$ dependence exhibits an additional maximum at $T_\mathrm{t} \simeq 125\,\mathrm{K}$ together with the anomaly at 140 K. The high temperature anomaly at $T_\mathrm{N} \simeq 140\,\mathrm{K}$ well agrees with the results of DC magnetic measurements data [17, 23]. However, the low temperature anomaly at $T_\mathrm{t} \simeq 125\,\mathrm{K}$ clearly visible in our specific heat $C(T)$ data wasn't previously detected on the DC magnetic measurements [17].

The total specific heat of $Fe_{0.5}TiS_2$ can be represented as a sum of electronic, lattice and magnetic contributions $C_\mathrm{totat} = C_\mathrm{el} + C_\mathrm{lat} + C_\mathrm{mag}$. Assuming that the magnetic contribution is negligible at temperatures far above the Neel temperature ($T > 170\,\mathrm{K}$) one can estimate the nonmagnetic contribution $C_\mathrm{el} + C_\mathrm{lat}$ from the high temperature part of the specific heat curve $C(T)$ using the Debye approximation. We have calculated the lattice contribution to the total specific heat by using the same value $\Theta_\mathrm{D} = 404\,\mathrm{K}$ as was taken to describe the thermal expansion (*see above*). The Debye temperature Θ_D for $Fe_{0.5}TiS_2$ was estimated by taking into account $\Theta_\mathrm{D} = 270\,\mathrm{K}$ for $Fe_{0.5}TiSe_2$ [6] and the difference in molar masses and unit cell volumes as was made in Ref. [24]. For the electronic contribution C_el, we used $\gamma = 7.4\,\mathrm{mJ\,mole^{-1}\,K^{-2}}$. The calculated curve $C_\mathrm{el} + C_\mathrm{lat}$ vs T is plotted by the dashed line in Fig. 5. The estimated values of γ and Θ_D for $Fe_{0.5}TiS_2$ are well within the range as observed for other transition metal dichalcogenides intercalated by $3d$-transition metals [25].

The neutron diffraction patterns observed for $Fe_{0.5}TiS_2$ within the temperature range between T_N and T_t and below T_t rule out the possibility of the ferromagnetic ground state suggested in Ref. [3, 26]. In order to find the possible spin configurations compatible with the lattice symmetry the representation analysis has been performed by means of the SARAh program [18]. For Fe magnetic ions occupying $2a$ Wyckoff site of the $I12/m1$

Table 1: Details on the magnetic structure representation analysis for $2a$ Wyckoff site of the space group $I12/m1$ and propagation vectors $\mathbf{k} = (\mu, 0, \nu)$ and $\mathbf{k} = (1/2, 0, 1/2)$.

IR	BV for $\mathbf{k} = (\mu, 0, \nu)$	IR	BV for $\mathbf{k} = (1/2, 0, 1/2)$
$\Gamma_1^{(1)}$	$\mathbf{\Psi}_1 = (0, 2, 0)$	$\Gamma_1^{(1)}$	$\mathbf{\Psi}_1 = (0, 4, 0)$
$\Gamma_2^{(1)}$	$\mathbf{\Psi}_2 = (2, 0, 0)$ $\mathbf{\Psi}_2 = (0, 0, 2)$	$\Gamma_3^{(1)}$	$\mathbf{\Psi}_1 = (4, 0, 0)$ $\mathbf{\Psi}_1 = (0, 0, 4)$

space group and propagation vector $\mathbf{k} = (\mu, 0, \nu)$, where μ and ν are incommensurate ones (or commensurate with $\mu = \nu = 0.25$), decomposition of magnetic representation of the propagation vector little group $G_{\mathbf{k}}$ gives two one-dimensional irreducible representations (IR) $\Gamma_{\text{Mag}} = \Gamma_1^{(1)} + 2\Gamma_2^{(1)}$. In the case of AFM structure with $\mathbf{k} = (1/2, 0, 1/2)$ decomposition gives two one-dimensional irreducible representations $\Gamma_{\text{Mag}} = \Gamma_1^{(1)} + 2\Gamma_3^{(1)}$. The corresponding basis vectors (BV) associated with the abovementioned irreducible representations are summarized in Table 1.

Such a magnetic structure of a spin-density-wave (SDW) type exhibit magnetic moments directed along the b direction for the irreducible representation $\Gamma_1^{(1)}$ while $\Gamma_2^{(1)}$ corresponds to the magnetic structure with moments aligned within the ac crystallographic plane, which is a mirror plane for Wyckoff $2a$ site. The Rietveld refinement has been performed for the high temperature ICM ($T = 130\,\text{K}$) and low temperature locked-in ($T = 2\,\text{K}$, $110\,\text{K}$) magnetic structures for both $\Gamma_1^{(1)}$ and $\Gamma_2^{(1)}$ irreducible representations. The best-fit results for all temperatures have been obtained for a model of the SDW-type structure with magnetic moments aligned within the ac plane of the irreducible representation $\Gamma_2^{(1)}$. The refined NPD patterns at $110\,\text{K}$ and $130\,\text{K}$ are shown in Figs. 6(a) and (b) while the details of that refinement are given in Table 2.

In order to study the magnetic field effect on the low temperature antiferromagnetic state of $Fe_{0.5}TiS_2$ two NPD patterns were measured after the sample was subjected to the field cooling (FC) procedure. The first NPD ($I^{\text{FC}}_{28\,\text{kOe}}$) was measured right after field cooling from $150\,\text{K}$ down to $2\,\text{K}$ in the applied field $28\,\text{kOe}$, which was maximal value accessible in our experi-

Table 2: Details on the Rietveld refinement of the magnetic structure for $Fe_{0.5}TiS_2$ at $T = 2\,K$, $110\,K$ and $130\,K$. The refined Fourier coefficients $\mathbf{S_k}$ are given in accordance with the propagation vector formalism for magnetic structure representation.

Temp	IR	$\mathbf{S_k} = \sum_n C_n \mathbf{\Psi}_n$	Discrepancy factors
$2\,K$	$\Gamma_2^{(1)}$	$0.52\mathbf{\Psi}_2 + 2.06\mathbf{\Psi}_3$	$R_B(\mathrm{Mag}) = 8.3$ $\chi^2 = 10.7$
$110\,K$	$\Gamma_2^{(1)}$	$0.52\mathbf{\Psi}_2 + 1.95\mathbf{\Psi}_3$	$R_B(\mathrm{Mag}) = 8.2$ $\chi^2 = 8.9$
$130\,K$	$\Gamma_2^{(1)}$	$0.44\mathbf{\Psi}_2 + 1.05\mathbf{\Psi}_3$	$R_B(\mathrm{Mag}) = 17.3$ $\chi^2 = 7.3$

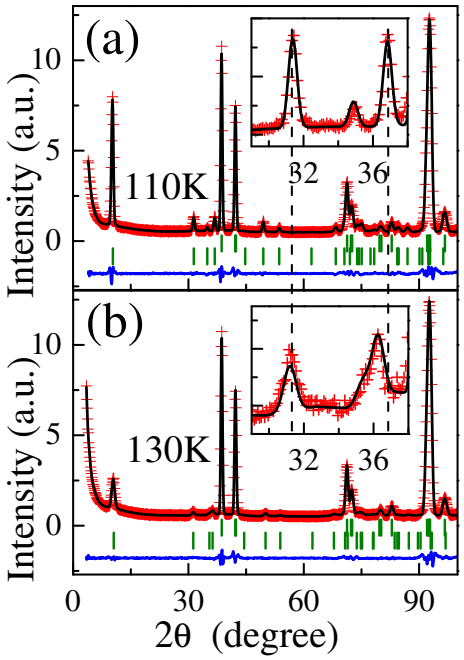

Figure 6: (Colour on-line) The best fit result for the NPD patterns measured below the Neel temperature at (a) $T = 110\,K$ and (b) $T = 130\,K$ for $Fe_{0.5}TiS_2$ sample. The insets show the temperature effect on the AFM reflections around $2\theta = 34°$.

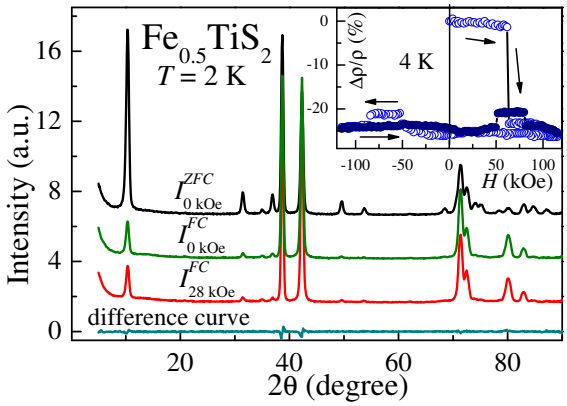

Figure 7: (Colour on-line) NPD patterns measured right after field cooling in applied magnetic field 28 kOe ($I^{\rm FC}_{28\,\rm kOe}$), after field cooling in zero magnetic field ($I^{\rm FC}_{0\,\rm kOe}$), their difference curve ($I^{\rm FC}_{28\,\rm kOe} - I^{\rm FC}_{0\,\rm kOe}$) and reference pattern measured after zero field cooling ($I^{\rm ZFC}_{0\,\rm kOe}$). The magnetoresistance isotherm $\frac{\Delta\rho}{\rho}(H)$ measured at $T = 4$ K [17] is shown in the inset.

ment. Then the magnetic field was switched off to zero and the second NPD pattern ($I^{\rm FC}_{0\,\rm kOe}$) was recorded at the same temperature. Both the neutron diffraction patterns, the difference curve ($I^{\rm FC}_{28\,\rm kOe} - I^{\rm FC}_{0\,\rm kOe}$) and the reference NPD pattern ($I^{\rm ZFC}_{0\,\rm kOe}$) measured at $T = 2$ K after zero-field cooling (ZFC) procedure are shown in Fig. 7. As can be clear seen, the $I^{\rm FC}_{28\,\rm kOe}$ pattern exhibits substantially suppressed AFM peaks in comparison with $I^{\rm ZFC}_{0\,\rm kOe}$ for the sample cooled in zero field. Incomplete suppression of the AFM peaks observed at 2 K after field cooling procedure is associated with retention of the AFM state in some number of particles with easy magnetization axis oriented nearly perpendicular to the field direction. As it turned out, switching off the 28 kOe field at $T = 2$ K does not restore the intensity of the AFM reflections. These results indicate the irreversibility of the field-induced AFM–FM transition in $Fe_{0.5}TiS_2$, which is consistent with irreversible behavior of the magnetoresistance (shown in the inset in Fig. 7).

An additional observation of the field-induced metamagnetic AFM–FM transition has been performed for the high temperature ICM phase. A series of neutron diffraction patterns has been measured in applied magnetic fields up to 28 kOe after zero field cooling from 160 K down to 130 K (see Fig. 8(a)). A drastic rise of the nuclear Bragg peak intensity around critical field $H_c \simeq 10$ kOe as a result of ferromagnetic contribution can be observed on Fig. 8(b). Along with appearance of the ferromagnetic contri-

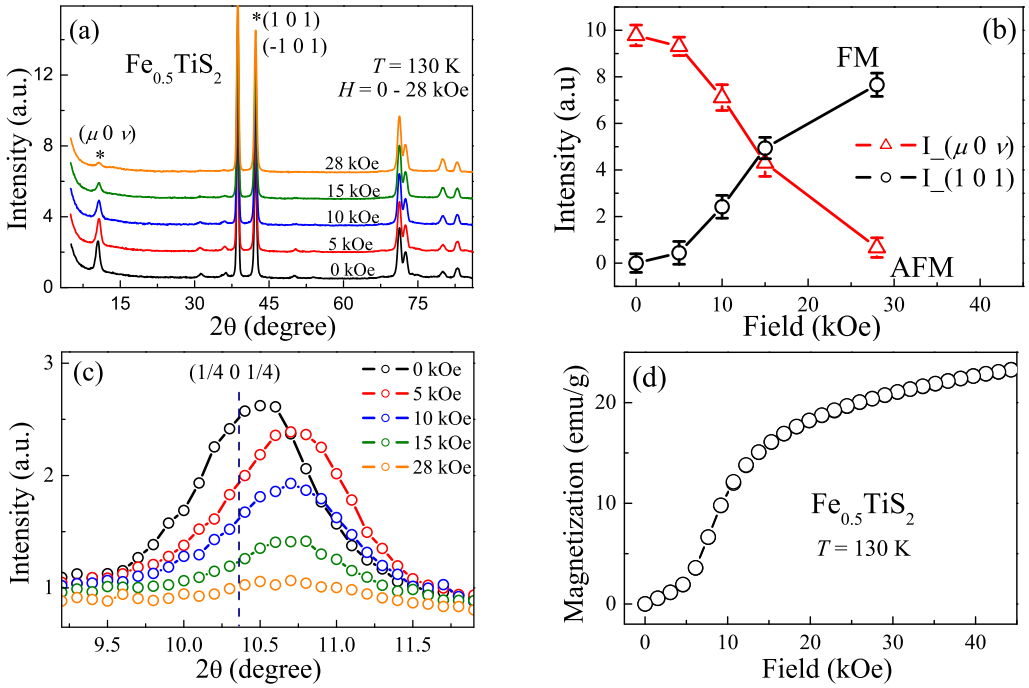

Figure 8: (Colour on-line) (a) Evolution of the NPD patterns measured at $T = 130\,\mathrm{K}$ for $Fe_{0.5}TiS_2$ upon application of the external magnetic field up to 28 kOe. (b) Integral intensities of the AFM satellite $(\mu\,0\,\nu)$ and FM contribution to the $(1\,0\,1)$ nuclear Bragg peak [both are marked by $(*)$ at figure 8 (a)] plotted as functions of applied magnetic field. (c) Enlarged part of the NPD patterns around $2\theta \simeq 10.50^\circ$ measured at $T = 130\,\mathrm{K}$ showing the magnetic field effect on the intensity and angle position of the AFM satellite $(\mu\,0\,\nu)$. (d) Magnetization curve measured at $T = 130\,\mathrm{K}$ on the polycrystalline $Fe_{0.5}TiS_2$ sample taken from Ref. [17].

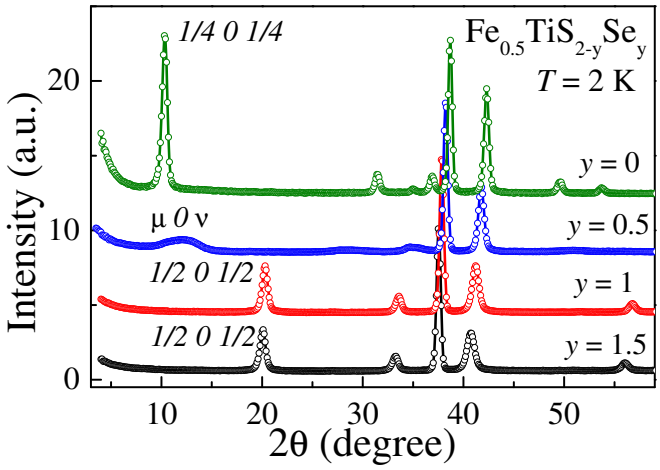

Figure 9: (Colour on-line) Evolution of the propagation vector upon substitution of Se for S as evidenced by the change of angle positions of magnetic peaks at the NPD patterns measured at $T = 2\,\mathrm{K}$.

bution an external magnetic field suppresses the AFM satellites and moves their angle positions away from the ones defined by CM propagation vector $\mathbf{k} = (0.25, 0, 0.25)$ (see the dashed line in Fig. 8(c)). Such a behavior well agrees with the field dependence of magnetization measured on a polycrystalline sample in applied magnetic fields up to 70 kOe (see Fig. 8(d)) and suggests a field induced AFM–FM transition for the high temperature ICM phase of $Fe_{0.5}TiS_2$.

3.3. Magnetic structure of substituted $Fe_{0.5}TiS_{2-y}Se_y$ compounds

Let us discuss the effect of the substitution of Se for S on the magnetic state of $Fe_{0.5}TiS_{2-y}Se_y$ compounds. Neutron diffraction patterns for $Fe_{0.5}TiS_{2-y}Se_y$ compounds with $y = 0, 0.5, 1, 1.5$ measured at $T = 2\,\mathrm{K}$ are shown in Fig. 9. As one can see the substitution of Se for S up to concentration $y_c = 0.5$ suppresses the narrow magnetic satellites indexed by propagation vector $\mathbf{k} = (0.25, 0, 0.25)$ and results in appearance of a broad (in comparison with the nuclear Bragg reflections) diffuse maxima. Such a behavior can be associated with the suppression of the long-range antiferromagnetic order and formation of the antiferromagnetically ordered magnetic clusters which do not transform to a long-range AFM order and persist down to the lowest temperature $T = 2\,\mathrm{K}$ accessible in our experiment. The propagation vector of the short-range antiferromagnetic order for

Table 3: Details on the Rietveld refinement of the magnetic structure for $Fe_{0.5}TiS_{2-y}Se_y$ ($y = 0, 0.5, 1, 1.5, 2$) at $T = 2\,K$. The refined Fourier coefficients $\mathbf{S_k}$ are given in accordance with the propagation vector formalism for magnetic structure representation.

Concentration	Propagation vector	Solution (IR)	$\mathbf{S_k} = \sum_n C_n \mathbf{\Psi}_n$	Discrepancy factors
$y = 0$	$\mathbf{k} = (0.25, 0, 0.25)$	$\Gamma_2^{(1)}$	$0.52\mathbf{\Psi}_2 + 2.06\mathbf{\Psi}_3$	$R_B(\text{Mag}) = 8.3$ $\chi^2 = 10.7$
$y = 0.5$	$\mathbf{k} = (0.31, 0, 0.27)$	$\Gamma_2^{(1)}$	$0.79\mathbf{\Psi}_2 + 1.68\mathbf{\Psi}_3$	$R_B(\text{Mag}) = 15.2$ $\chi^2 = 12.8$
$y = 1.0$	$\mathbf{k} = (1/2, 0, 1/2)$	$\Gamma_3^{(1)}$	$0.21\mathbf{\Psi}_2 + 0.76\mathbf{\Psi}_3$	$R_B(\text{Mag}) = 8.0$ $\chi^2 = 18.2$
$y = 1.5$	$\mathbf{k} = (1/2, 0, 1/2)$	$\Gamma_3^{(1)}$	$0.22\mathbf{\Psi}_2 + 0.77\mathbf{\Psi}_3$	$R_B(\text{Mag}) = 8.9$ $\chi^2 = 24.7$
$y = 2.0$	$\mathbf{k} = (1/2, 0, 1/2)$	$\Gamma_3^{(1)}$	$0.22\mathbf{\Psi}_2 + 0.77\mathbf{\Psi}_3$	$R_B(\text{Mag}) = 11.2$ $\chi^2 = 6.8$

$Fe_{0.5}TiS_{1.5}Se_{0.5}$ has been roughly estimated at $T = 2\,K$ as an incommensurate one $\mathbf{k} = (0.31, 0, 0.27)$. An increase of the Se content up to $y = 1$ results in recovery of the long-range antiferromagnetic order with the commensurate propagation vector $\mathbf{k} = (1/2, 0, 1/2)$. A further rise of the Se content up to $y = 1.5$ and $y = 2$ [6] doesn't affect the magnetic structure. The Rietveld refinement of the low temperature $T = 2\,K$ neutron diffraction patterns for $Fe_{0.5}TiS_{2-y}Se_y$ compounds with $y = 0.5, 1, 1.5$ revealed that the best fit result was obtained for the magnetic moments aligned within the crystallographic plane ac i.e. for $\Gamma_2^{(1)}$ irreducible representation of the ICM structure with $\mathbf{k} = (0.31, 0, 0.27)$ and for $\Gamma_3^{(1)}$ irreducible representation of the CM structure with $\mathbf{k} = (1/2, 0, 1/2)$ (see Table 1). The details on the Rietveld refinement for $Fe_{0.5}TiS_{2-y}Se_y$ with ($y = 0, 0.5, 1, 1.5, 2$) compounds at $T = 2\,K$ are specified in Table 3. Having a and c components of the Fourier coefficients $\mathbf{S_k}$ from Table 3 one can estimate that the Fe magnetic moments make an angle of $14^\circ - 16^\circ$ with c crystallographic direction for all the $Fe_{0.5}TiS_{2-y}Se_y$ compounds.

4. Summary and conclusion

In the present work a detailed study of the crystal structure and magnetic state of $Fe_{0.5}TiS_{2-y}Se_y$ compounds with $y = 0, 0.5, 1, 1.5, 2$ has been performed by means of powder neutron diffraction. It has been found that all the studied compounds crystallize in the layered $a_0\sqrt{3} \times a_0 \times 2c_0$ superstructure (space group $I12/m1$). The substitution of Se for S results in the expected growth of the lattice parameters and unit cell volume due to the difference in the ionic radii of S and Se. As $Fe_{0.5}TiSe_2$ [6], the Fe intercalated titanium disulfide is found to exhibit anisotropic magnetoelastic deformations below the Neel temperature while the temperature variation of the unit cell volume follows to the Grüneisen-Debye theory. Among the other compounds, $Fe_{0.5}TiS_2$ is of a particular interest due to its complex underlying magnetic state which was suggested to be ferromagnetic [3, 26], antiferromagnetic [17, 23] or antiferromagnetic with the inclusion of ferromagnetic clusters [27]. However, our neutron diffraction measurements performed in a wide temperature range together with the specific heat measurements have shown that this compound enters an incommensurate antiferromagnetic order with cooling below the Neel temperature $T_N \simeq 140\,K$ and exhibits a magnetic phase transition to the lock-in phase on cooling below $T_t \simeq 125\,K$. The presence of two magnetic phase transitions at $T_N \simeq 140\,K$ and $T_t \simeq 125\,K$ in $Fe_{0.5}TiS_2$ is clear evidenced by specific heat measurements. For the temperature interval $T_t < T < T_N$, the incommensurate magnetic structure of the SDW type can be described by the propagation vector $\mathbf{k} = (\mu, 0, \nu)$, where $\mu = 0.26$ and $\nu = 0.23$, while below $T_t \simeq 125\,K$, the magnetic structure of $Fe_{0.5}TiS_2$ is commensurate with the propagation vector $\mathbf{k} = (0.25, 0, 0.25)$.

The neutron diffraction measurements under an applied magnetic field performed in both temperature intervals $T_t < T < T_N$ and below $T_t \simeq 125\,K$ have revealed that the magnetic field induces a magnetic phase transition from the AFM to FM state. The inducement of the FM state in $Fe_{0.5}TiS_2$ is found to be irreversible below 110 K, which is evidenced by our NPD measurements performed on the field cooled sample and after switching off the field. It should be noted, that the irreversible field-induced transitions from AFM to FM state have been reported for some other antiferromagnets, in particular, for rare-earth – transition metal intermetallic compounds (R_3Co (R=Dy, Ho) [28, 29], $Ce(Fe_{1-x}Co_x)_2$ [30], Gd_5Ge_4 [31]), Nd_7Rh_3 [32]), for Pr-doped manganites [33], for transition-metal-based compounds (Fe(Rh,Pd) [34], $(Mn,Co)_2Sb$ [35], $La(Fe_xAl_{1-x})_{13}$ [36]) and for molecule-

based magnets (see Ref. [37], for instance). The measurements of the thermal expansion or forced magnetostriction performed for such type of materials have revealed that spontaneous or field-induced AFM–FM transitions are accompanied by an appreciable magnetovolume effect which influences the hysteresis behavior at the transitions. A substantial role of the magnetoelastic interactions in the first-order AFM–FM transition was also derived from theoretical considerations within local-moment [38] or itinerant-magnetism [39] models. In $Fe_{0.5}TiS_2$, application of an external magnetic field below T_N induces the AFM–FM metamagnetic transition which should affect the exchange interaction energy and produce the changes in the interatomic distances as in above mentioned materials. As a result, a local minimum should appear in the free energy which includes the distance-dependent exchange, magnetocrystalline anisotropy, magnetic field and lattice deformation contributions. One can suggest that the presence of such a local minimum and energy barrier is responsible for the persistence of the field-induced metastable FM state observed in $Fe_{0.5}TiS_2$. Unfortunately, we could not detect the changes in the structural parameters at the AFM–FM transition using the DMC diffractometer probably because of a low magnetovolume effect. Further studies are needed in order to confirm the irreversible changes in the unit cell volume at AFM–FM transition in this compound.

NPD measurements performed for the substituted $Fe_{0.5}TiS_{2-y}Se_y$ compounds confirm the presence of low temperature AFM states below T_N within the whole S-Se concentration range. At $y > 0.5$, the additional magnetic phase transformations in magnetically ordered state were not detected. The substitution of isoelectronic Se for S is observed to result in the transition from the AFM structure with quadruplicated magnetic unit cell $\mathbf{k} = (0.25, 0, 0.25)$ via a short-range correlated magnetic state around the critical concentration of $y_c = 0.5$ with ICM structure of SDW-type $\mathbf{k} = (0.31, 0, 0.27)$ to the AFM structure with magnetic unit cell doubled along the a and c crystallographic directions $\mathbf{k} = (0.5, 0, 0.5)$. Bearing in mind that sulfur and selenium have the same valences, but different ionic radii one can suggest that the main force of the observed concentration induced changes in the arrangement of Fe magnetic moments in $Fe_{0.5}TiS_{2-y}Se_y$ is the sensitivity of the exchange interaction to the interatomic distances. The Rietveld refinement of the low temperature magnetic structure for $Fe_{0.5}TiS_{2-y}Se_y$ compounds revealed the AFM structure with magnetic moments aligned within the ac crystallographic plane making an angle of $14^\circ - 16^\circ$ with c crystallographic direction. Contrary to the magnetic

structure of $Fe_{0.5}TiS_{2-y}Se_y$ compounds exhibiting monoclinically distorted NiAs-type unit cell the magnetic moments of the Fe_xTX_2 type compounds with nondistorted hexagonal unit cell are aligned strictly along the c crystallographic axis [40]. Thus one can suggest that the crystal electric field effect along with the spin-orbital interaction of distorted chalcogen octahedrons may be an origin of the magnetic moments inclination from the c crystallographic axis for $Fe_{0.5}TiS_{2-y}Se_y$ compounds.

In conclusion, in the present work we have shown how the selenium for sulfur substitution influences the magnetic order in the subsystem of Fe atoms intercalated into mixed titanium dichalcogenide $TiS_{2-y}Se_y$. By using neutron powder diffraction measurements all the $Fe_{0.5}TiS_{2-y}Se_y$ compounds ($0 \leq y \leq 2$) are classified as having an antiferromagnetic ground state. The growth of the Se concentration in $Fe_{0.5}TiS_{2-y}Se_y$ is accompanied by expansion of the crystal lattice and by changes in the periodicity of the arrangement of Fe magnetic moments at low temperatures from quadruplicated (at $y < 0.5$) to doubled (at $y > 0.5$) magnetic unit cell along the a and c axes in respect to the crystal lattice. Despite such evolutions of the magnetic structure associated with variations in the distance-dependent exchange interactions the local easy axes directions of Fe magnetic moments remain almost unchanged upon the S-Se substitution. The orientation of Fe moments within the ac plane at an angle of about 15° is suggested to be controlled by crystal fields and spin-orbital interactions. The permanent magnet properties and a high coercitivity (H_c up 50 kOe) of the antiferromagnetic compound Fe_xTX_2 are realized in the field-induced FM state which is metastable as evidenced by NPD measurements. Further studies are needed in order to answer the question about the value of the Fe orbital moment and origins of the irreversibility of the field-induced AFM–FM transformations in $Fe_{0.5}TiS_{2-y}Se_y$ with low ($y < 0.5$) Se concentrations.

Acknowledgments

This work is partly based on experiments performed at the Swiss spallation neutron source SINQ, Paul Scherrer Institute, Villigen, Switzerland. This work was supported by the Russian Foundation for Basic Research (projects No 13-02-00364 and 14-02-92104) and by the program of the Ural Branch of RAS (project No 12-T-2-1012).

References

[1] M. Inoue, H. Hughes, A. Yoffe, The electronic and magnetic properties of the 3d transition metal intercalates of TiS_2, Adv. Phys. 38 (1989) 565–604. doi:10.1080/00018738900101142.

[2] S. S. P. Parkin, R. H. Friend, 3d transition-metal intercalates of the niobium and tantalum dichalcogenides. I. Magnetic properties, Phylos. Mag. B 41 (1980) 65–93. doi:10.1080/13642818008245370.

[3] H. Negishi, A. Shoube, H. Takahashi, Y. Ueda, M. Sasaki, M. Inoue, Magnetic properties of intercalation compounds M_xTiS_2 (M = 3d transition metal), J. Magn. Magn. Mat. 67 (1987) 179 – 186. doi:10.1016/0304-8853(87)90227-7.

[4] Y. Tazuke, Y. Ohta, S. Miyamoto, Exchange interactions in Fe_xTiS_2, J. Phys. Soc. Jpn. 74 (2005) 2644–2645. doi:10.1143/JPSJ.74.2644.

[5] K.-T. Ko, K. Kim, S. B. Kim, H.-D. Kim, J.-Y. Kim, B. I. Min, J.-H. Park, F.-H. Chang, H.-J. Lin, A. Tanaka, S.-W. Cheong, RKKY ferromagnetism with Ising-like spin states in intercalated $Fe_{0.25}TaS_2$, Phys. Rev. Lett. 107 (2011) 247201. doi:10.1103/PhysRevLett.107.247201.

[6] N. Selezneva, N. Baranov, V. Pleshchev, N. Mushnikov, V. Maksimov, Magnetic state and properties of the $Fe_{1/4}TiSe_2$ intercalation compound, Phys. Solid State 53 (2011) 329–336. doi:10.1134/S1063783411020272.

[7] T. Miyadai, K. Kikuchi, H. Kondo, S. Sakka, M. Arai, Y. Ishikawa, Magnetic properties of $Cr_{1/3}NbS_2$, J. Phys. Soc. Jpn. 52 (1983) 1394–1401. doi:10.1143/JPSJ.52.1394.

[8] F. Hulliger, E. Pobitschka, On the magnetic behavior of new 2H-NbS_2 type derivatives, J. Solid State Chem. 1 (1970) 117 – 119. doi:10.1016/0022-4596(70)90001-0.

[9] Y. Togawa, T. Koyama, K. Takayanagi, S. Mori, Y. Kousaka, J. Akimitsu, S. Nishihara, K. Inoue, A. S. Ovchinnikov, J. Kishine, Chiral magnetic soliton lattice on a chiral helimagnet, Phys. Rev. Lett. 108 (2012) 107202. doi:10.1103/PhysRevLett.108.107202.

[10] N. V. Baranov, A. N. Titov, V. I. Maksimov, N. V. Toporova, A. Daoud-Aladine, A. Podlesnyak, Antiferromagnetism in the ordered subsystem of Cr ions intercalated into titanium diselenide, J. Phys.: Condens. Matter 17 (2005) 5255. doi:10.1088/0953-8984/17/34/010.

[11] N. V. Baranov, V. G. Pleshchev, N. V. Selezneva, E. M. Sherokalova, A. V. Korolev, V. A. Kazantsev, A. V. Proshkin, Ferromagnetism and structural transformations caused by Cr intercalation into $TiTe_2$, J. Phys.: Condens. Matter 21 (2009) 506002. doi:10.1088/0953-8984/21/50/506002.

[12] A. F. Kusmartseva, B. Sipos, H. Berger, L. Forró, E. Tutiš, Pressure induced superconductivity in pristine 1T-$TiSe_2$, Phys. Rev. Lett. 103 (2009) 236401. doi:10.1103/PhysRevLett.103.236401.

[13] B. Sipos, A. F. Kusmartseva, A. Akrap, H. Berger, L. Forró, E. Tutiš, From Mott state to superconductivity in 1T-TaS_2, Nat. Mater. 7 (2008) 960–965. doi:10.1038/nmat2318.

[14] M. Inoue, M. Koyano, K. Fukushima, H. Negishi, M. Sasaki, Pressure dependence of electrical resistivity in intercalation compounds M_xTiS_2 (M = 3d transition metal), Phys. Status Solidi (b) 139 (1987) 273–280. doi:10.1002/pssb.2221390126.

[15] K. Nagao, M. Koyano, S. Katayama, Y. Yamamura, T. Tsuji, Raman scattering from intercalation compounds Fe_xNbS_2 under high pressure, Phys. Status Solidi (b) 223 (2001) 281–285. doi:10.1002/1521-3951(200101)223:1¡281::AID-PSSB281¿3.0.CO;2-Z.

[16] N. Barišić, I. Smiljanić, P. Popčević, A. Bilušić, E. Tutiš, A. Smontara, H. Berger, J. Jaćimović, O. Yuli, L. Forró, High-pressure study of transport properties in $Co_{0.33}NbS_2$, Phys. Rev. B 84 (2011) 075157. doi:10.1103/PhysRevB.84.075157.

[17] N. V. Baranov, E. M. Sherokalova, N. V. Selezneva, A. V. Proshkin, A. F. Gubkin, L. Keller, A. S. Volegov, E. P. Proskurina, Magnetic order, field-induced phase transitions and magnetoresistance in the intercalated compound $Fe_{0.5}TiS_2$, J. Phys.: Condens. Matter 25 (2013) 066004. doi:10.1088/0953-8984/25/6/066004.

[18] A. Wills, A new protocol for the determination of magnetic structures using simulated annealing and representational analysis $SARAh$, Physica B 276278 (2000) 680 – 681. doi:10.1016/S0921-4526(99)01722-6.

[19] J. Rodríguez-Carvajal, Recent advances in magnetic structure determination by neutron powder diffraction, Physica B 192 (1993) 55 – 69. doi:10.1016/0921-4526(93)90108-I.

[20] G. Calvarin, J. Gavarri, M. A. Buhannic, P. Colombet, M. Danot, Crystal and magnetic structures of $Fe_{0.25}TiSe_2$ and $Fe_{0.48}TiSe_2$, Rev. Phys. Appl. 22 (1987) 1131–1138. doi:10.1051/rphysap:0198700220100113100.

[21] R. H. Plovnick, M. Vlasse, A. Wold, Preparation and structural properties of some ternary chalcogenides of titanium, Inorg. Chem. 7 (1968) 127–129. doi:10.1021/ic50059a026.

[22] M. Buhannic, P. Colombet, M. Danot, G. Calvarin, The iron electronic characteristics and the crystal dimensionality of the phases Fe_xTiSe_2 ($x = 0.25, 0.38, 0.50$), J. Solid State Chem. 69 (1987) 280 – 288. doi:10.1016/0022-4596(87)90085-5.

[23] S. Muranaka, Magnetic properties of $FeTi_2S_4$, J. Phys. Soc. Jpn. 35 (1973) 616–616. doi:10.1143/JPSJ.35.616.

[24] N. V. Baranov, H. Michor, G. Hilscher, A. Proshkin, A. Podlesnyak, Extra T-linear specific heat contribution induced by the f-d exchange in Gd-Ni binary compounds, J. Phys.: Condens. Matter 20 (2008) 325233. doi:10.1088/0953-8984/20/32/325233.

[25] M. Inoue, Y. Muneta, H. Negishi, M. Sasaki, Specific heat measurements of intercalation compounds M_xTiS_2 (M=3d transition metals) using ac calorimetry technique, J. Low. Temp. Phys. 63 (1986) 235–245. doi:10.1007/BF00683766.

[26] T. Satoh, Y. Tazuke, T. Miyadai, K. Hoshi, Ferromagnetic and reentrant spin glass properties in an ising magnet Fe_xTiS_2, J. Phys. Soc. Jpn. 57 (1988) 1743–1750. doi:10.1143/JPSJ.57.1743.

[27] B. L. Morris, V. Johnson, R. H. Plovnick, A. Wold, Magnetic properties of $FeTi_2S_4$, J. Appl. Phys. 40 (1969) 1299–1300. doi:10.1063/1.1657639.

[28] N. Baranov, A. Pirogov, A. Teplykh, Magnetic state of Dy_3Co, J. Alloys Comp. 226 (1995) 70 – 74. doi:10.1016/0925-8388(95)01574-4.

[29] N. V. Baranov, T. Goto, G. Hilscher, P. E. Markin, H. Michor, N. V. Mushnikov, J.-G. Park, A. A. Yermakov, Irreversible field-induced magnetic phase transitions and properties of Ho_3Co, J. Phys.: Condens. Matter 17 (2005) 3445. doi:10.1088/0953-8984/17/21/034.

[30] H. Fukuda, H. Fujii, H. Kamura, Y. Hasegawa, T. Ekino, N. Kikugawa, T. Suzuki, T. Fujita, Magnetic and transport properties of the pseudobinary systems $Ce(Fe_{1-x}Co_x)_2$ and $(Ce_{1-y}Sc_y)Fe_2$, Phys. Rev. B 63 (2001) 054405. doi:10.1103/PhysRevB.63.054405.

[31] M. K. Chattopadhyay, M. A. Manekar, A. O. Pecharsky, V. K. Pecharsky, K. A. Gschneidner, J. Moore, G. K. Perkins, Y. V. Bugoslavsky, S. B. Roy, P. Chaddah, L. F. Cohen, Metastable magnetic response across the antiferromagnetic to ferromagnetic transition in Gd_5Ge_4, Phys. Rev. B 70 (2004) 214421. doi:10.1103/PhysRevB.70.214421.

[32] T. Tsutaoka, K. Shimomura, A. Tanaka, Irreversible magnetovolume effect in Nd_7Rh_3 single crystal, J. Magn. Magn. Mat. 323 (2011) 3147 – 3150. doi:10.1016/j.jmmm.2011.06.075.

[33] J. Dho, N. H. Hur, Thermal relaxation of field-induced irreversible ferromagnetic phase in Pr-doped manganites, Phys. Rev. B 67 (2003) 214414. doi:10.1103/PhysRevB.67.214414.

[34] N. Baranov, E. Barabanova, Electrical resistivity and magnetic phase transitions in modified FeRh compounds, J. Alloys Comp. 219 (1995) 139 – 148. doi:10.1016/0925-8388(94)01375-6.

[35] M. Bartashevich, T. Goto, T. Tomita, N. Baranov, S. Zemlyanski, G. Hilscher, H. Michor, AF–FRI metamagnetic transition in itinerant $Mn_{2-x}Co_xSb$ system: high-field and high-pressure effects, Physica B 318 (2002) 198 – 210. doi:10.1016/S0921-4526(01)01471-5.

[36] K. Irisawa, A. Fujita, K. Fukamichi, M. Yamada, H. Mitamura, T. Goto, K. Koyama, Transition between antiferromagnetic and ferromagnetic states in itinerant-electron $La(Fe_xAl_{1-x})_{13}$ compounds, Phys. Rev. B 70 (2004) 214405. doi:10.1103/PhysRevB.70.214405.

[37] Y. Numata, K. Inoue, N. Baranov, M. Kurmoo, K. Kikuchi, Field-induced ferrimagnetic state in a molecule-based magnet consisting of a Co^{II} ion and a chiral triplet bis(nitroxide) radical, J. Am. Chem. Soc. 129 (2007) 9902–9909. doi:10.1021/ja064828i.

[38] J. H. V. J. Brabers, K. H. J. Buschow, F. R. de Boer, Field-induced first-order antiferromagnetic-ferromagnetic transitions in RMn_2Ge_2 compounds and their relation to the magnetostriction of the Mn sublattice, Phys. Rev. B 59 (1999) 9314–9323. doi:10.1103/PhysRevB.59.9314.

[39] A. Hernando, J. Barandiarán, J. Rojo, J. Gómez-Sal, About the effect of pressure and volume expansion on the transition from antiferromagnetic to ferromagnetic state in some metal alloys, J. Magn. Magn. Mat. 174 (1997) 181 – 184. doi:10.1016/S0304-8853(97)00216-3.

[40] B. V. Laar, H. Rietveld, D. Ijdo, Magnetic and crystallographic structures of Me_xNbS_2 and Me_xTaS_2, J. Sol. State Chem. 3 (1971) 154 – 160. doi:10.1016/0022-4596(71)90019-3.